Guo *et al. Diagnostic Pathology* (2025) 20:28
https://doi.org/10.1186/s13000-025-01621-6

Diagnostic Pathology

RESEARCH Open Access

Advanced pathological subtype classification of thyroid cancer using efficientNetB0

Hongpeng Guo[1†], Junjie Zhang[2†], You Li[1], Xinghe Pan[1*] and Chenglin Sun[1*]

Abstract

Background Thyroid cancer is a prevalent malignancy requiring accurate subtype identification for effective treatment planning and prognosis evaluation. Deep learning has emerged as a valuable tool for analyzing tumor microenvironment features and distinguishing between pathological subtypes, yet the interplay between microenvironment characteristics and clinical outcomes remains unclear.

Methods Pathological tissue slices, gene expression data, and protein expression data were collected from 118 thyroid cancer patients with various subtypes. The data underwent preprocessing, and 10 AI models, including EfficientNetB0, were compared. EfficientNetB0 was selected, trained, and validated, with microenvironment features such as tumor-immune cell interactions and extracellular matrix (ECM) composition extracted from the samples.

Results The study demonstrated the high accuracy of the EfficientNetB0 model in differentiating papillary, follicular, medullary, and anaplastic thyroid carcinoma subtypes, surpassing other models in performance metrics. Additionally, the model revealed significant correlations between microenvironment features and pathological subtypes, impacting disease progression, treatment response, and patient prognosis.

Conclusion The research establishes the effectiveness of the EfficientNetB0 model in identifying thyroid cancer subtypes and analyzing tumor microenvironment features, providing insights for precise diagnosis and personalized treatment. The results enhance our understanding of the relationship between microenvironment characteristics and pathological subtypes, offering potential molecular targets for future treatment strategies.

Keywords Thyroid cancer, EfficientNetB0 algorithm model, Pathological subtype, Tumor microenvironment, Precise diagnosis, Personalized treatment

Introduction

Thyroid cancer is one of the most common malignancies of the endocrine system worldwide, with its incidence rising significantly over the past few decades [1–3]. Although its overall prognosis is favorable, there are significant differences in clinical presentation and biological behavior among pathological subtypes [4–6]. According to the 2022 WHO classification criteria, thyroid cancer is primarily categorized into papillary thyroid carcinoma (PTC), follicular thyroid carcinoma (FTC), medullary thyroid carcinoma (MTC), high-grade follicular-derived carcinomas, hürthle cell carcinoma (HTC), and

†Hongpeng Guo and Junjie Zhang are regarded as co-first authors.

*Correspondence:
Xinghe Pan
15384708888@163.com
Chenglin Sun
scl66661110@163.com
[1]Department of General Surgery, The Second Hospital Affiliated to Shenyang Medical College, No.64, Qishan West Road, Huanggu District, Shenyang, Liaoning 110002, China
[2]Department of Pathology, Central Hospital Affiliated to Shenyang Medical College, Shenyang, Liaoning 110024, China

anaplastic thyroid carcinoma (ATC) [4, 5, 7]. Classification is based on cellular morphology, immunohistochemical markers and specific diagnostic protocols.

PTC is the most common subtype (85–90%), characterized by distinctive nuclear characteristics such as nuclear grooves and intranuclear pseudoinclusions. Key markers include Cytokeratin 19 (CK19) and HBME-1, with BRAF V600E mutation detection aiding confirmation [8]. FTC, accounting for 10–15% of thyroid cancers, is distinguished by follicular growth patterns and capsular or vascular invasion, with a higher risk of distant metastasis [5]. Medullary carcinoma, though rare, originates from thyroid C cells and is diagnosed using calcitonin, carcinoembryonic antigen (CEA), and RET proto-oncogene mutations [4].

High-grade follicular-derived carcinomas exhibit significant aggressiveness and metastatic potential [5]. HTC, a subtype characterized by mitochondria-rich cells, requires microscopic examination of granular cytoplasm along with specialized staining and immunohistochemical analysis for confirmation. It has a poor prognosis with a high risk of local recurrence and distant metastasis [4]. ATC, the rarest and most aggressive type, originates from follicular cells. It is marked by p53 overexpression and a high Ki67 proliferation index, requiring sensitive pathological analysis due to its rapid progression and short survival period [7].

Accurate identification of these pathological subtypes is crucial for individualized treatment planning, improving patient survival rates and quality of life [8]. Therefore, rapid and precise classification of thyroid cancer subtypes remains a key focus of ongoing clinical and research efforts [9–11].

With the rapid development of artificial intelligence, deep learning has significantly improved medical imaging analysis. Models such as InceptionV4 and DenseNet201 have been applied to tumor classification, detection, and prognostic evaluation, enhancing accuracy and efficiency while reducing human errors [12–14]. However, the performance of different deep models in recognizing thyroid cancer subtypes requires further comparison and validation [15, 16]. Additionally, exploring deep learning applications in analyzing thyroid cancer's microenvironment could enhance diagnostic and therapeutic precision [17].

The tumor microenvironment, composed of tumor cells, immune cells, and the extracellular matrix (ECM), plays a key role in cancer progression and metastasis [18, 19]. Factors such as high PD-L1 expression and immune cell infiltration are linked to better immunotherapy responses and prognosis [20–24]. ECM density, particularly collagen fiber composition, influences tumor invasion and metastasis, though its relationship with thyroid cancer subtypes remains incompletely understood [25, 26]. Further investigation into these interactions and their impact on clinical outcomes is essential for optimizing thyroid cancer treatment strategies [4, 27, 28].

The tumor microenvironment, composed of tumor cells, immune cells, and the extracellular matrix (ECM), plays a key role in cancer progression and metastasis [18, 19]. Factors such as high PD-L1 expression and immune cell infiltration are linked to better immunotherapy responses and prognosis [20–24]. Additionally, ECM density, particularly collagen fiber composition, influences tumor invasion and metastasis, though its relationship with thyroid cancer subtypes remains incompletely understood [25, 26]. Further exploration of the interactions among these features and their impact on clinical outcomes will help optimize treatment strategies for thyroid cancer [4, 27, 28].

This study aims to validate the EfficientNetB0 model in distinguishing thyroid cancer subtypes and identifying key tumor microenvironment features. By examining their influence on clinical progression, treatment response, and prognosis, we seek to improve diagnostic precision and personalized treatment. A deeper understanding of these relationships will aid in developing comprehensive diagnostic criteria and treatment strategies, ultimately improving patient survival rates and quality of life. This has significant implications for both clinical practice and research.

Materials and methods

Collection of thyroid cancer samples

A total of 118 samples were collected from thyroid cancer patients, including both cancerous tissue and adjacent normal tissue, covering various pathological subtypes. Among these samples, there were 57 cases of PTC, 39 cases of FTC, 11 cases of MTC, and 11 cases of ATC. The thyroid cancer samples include pathological slides, gene expression data, and protein expression data.

Gene expression data were obtained using RNA extraction and RNA sequencing techniques (RNA-seq). Specifically, total RNA was extracted from each sample using TRIzol reagent for lysis and separation, followed by mRNA sequencing on a high-throughput platform (e.g., Illumina NovaSeq) to generate gene expression profiles. Data analysis was conducted using a standard bioinformatics workflow, which includes quality control, alignment to a reference genome, and quantification of expression levels. Protein expression data were obtained through mass spectrometry (MS) analysis. Initially, proteins were extracted from the samples, separated by SDS-PAGE, and digested with trypsin. Subsequently, peptides were separated and identified using liquid chromatography-tandem mass spectrometry (LC-MS/MS). Detected peptides were matched and quantified using protein database search algorithms, such as MaxQuant, to obtain protein expression profiles.

Definition and collection of clinical characteristics

Clinical characteristics for each patient include age, gender, pathological diagnosis results, and treatment history. These data were collected through the electronic medical record system. Tumor staging was assessed according to the 8th edition of the American Joint Committee on Cancer (AJCC) TNM staging system, and pathological subtypes were determined based on the 2022 WHO classification criteria for thyroid tumors. Detailed clinical characteristic data are listed in the supplementary table (Table S1).

Definition of treatment response

Treatment response was classified according to the Response Evaluation Criteria in Solid Tumors (RECIST 1.1) and includes the following categories: Complete Response (CR), defined as the disappearance of all target lesions, sustained for at least 4 weeks; Partial Response (PR), marked by a minimum 30% decrease in the sum of the diameters of target lesions, sustained for at least 4 weeks; Stable Disease (SD), where tumor lesions neither meet the criteria for CR nor for Progressive Disease (PD); and PD, characterized by at least a 20% increase in the sum of the diameters of target lesions or the appearance of new lesions. These treatment responses were confirmed through regular imaging evaluations and documented in the patients' treatment records.

Definition of prognosis

Prognosis was assessed using overall survival (OS) and progression-free survival (PFS). OS is defined as the time from diagnosis to death, while PFS is defined as the time from the start of treatment to disease progression or death. Follow-up information for all patients was obtained through the EMR system and telephone follow-ups, with a cut-off date of January 2024.

Data integration and cleaning

Utilize professional data processing software, such as Python's Pandas library, to preprocess the collected data (Figure S1). This process involves integrating and cleaning the pathological slide images, gene expression data, and protein expression data. Initially, it is essential to match and merge different data types for each sample to ensure data completeness. Subsequently, automated scripts are employed to detect and remove duplicate records, rectify erroneous data inputs, and address missing values utilizing appropriate methods, such as filling continuous variables with the mean and categorical variables with the mode.

Image preprocessing

Standardized preprocessing procedures were applied to pathological tissue slide images (Figure S2), involving resizing and color normalization, to ensure consistency for subsequent analysis. Gene and protein data, on the other hand, were normalized using specific bioinformatics tools, handling missing values and selecting meaningful data based on principles of biostatistics to prepare for subsequent feature selection and dimensionality reduction.

Feature selection and dimensionality reduction

In dealing with high-dimensional data, common methods such as Principal Component Analysis (PCA) and Linear Discriminant Analysis (LDA) are often employed to reduce the dimensionality of the data. By combining model-based feature selection and evaluating feature importance using the Random Forest algorithm, key features are identified. This step aims to decrease noise in the data, enhancing the accuracy and efficiency of subsequent analyses.

Algorithm model selection

Ten AI algorithm models, including InceptionV4, InceptionV3, EfficientNetB0, DenseNet201, DenseNet121, DarkNet Large, DarkNet Small, VGG19 BN, VGG19, and SEResNet50, were evaluated (Table S2) to determine the model most suitable for the characteristics of thyroid cancer data. Performance on preprocessed data, adaptability, and overall effectiveness were considered when selecting the optimal model. Preliminary testing and literature review were utilized to make the final decision.

Model training

During AI model training, the model learns to recognize various features within images to distinguish thyroid cancer cells from normal cells. These features include not only cell shape and size but also cell arrangement, nuclear density, and color distribution. Specifically, when processing thyroid cancer pathology images, the EfficientNetB0 model automatically captures key visual characteristics that aid in accurate classification.

Cell Morphology Features: Thyroid cancer cells often exhibit morphological differences from normal cells. The model identifies variations in nuclear size and shape, as cancerous thyroid cells typically have larger, irregularly shaped nuclei compared to normal cells. By learning these morphological features, the AI model can detect cellular abnormalities and predict the presence of cancer.

Cell Arrangement Patterns: In thyroid cancer tissues, cancer cells tend to cluster in irregular patterns, in contrast to the orderly arrangement seen in normal tissue. During training, the EfficientNetB0 model learns these structural patterns, enabling it to identify abnormal arrangements and distinguish cancerous areas from normal regions.

Color and Texture Features: Thyroid cancer cells often display distinct color and texture characteristics in pathological slides, particularly in nuclear-to-cytoplasmic ratios and nuclear staining density, which differ markedly from normal cells. The model can recognize these subtle color and texture variations, identifying cancerous tissue by detecting differences in staining intensity. For example, thyroid cancer tissue may show deeper staining with higher nuclear density, which the model interprets as indicative of malignancy.

In analyzing a pathology image containing a cluster of cells, models like EfficientNetB0 first scan the entire image, automatically detecting and marking potentially abnormal regions. The model then analyzes these regions by evaluating cell morphology, arrangement patterns, and staining characteristics, ultimately integrating these features to determine whether a region is cancerous. For instance, if the model detects enlarged nuclei and high staining intensity within a cellular area, it may classify this region as likely harboring cancer cells.

In simple terms, the EfficientNetB0 model operates similarly to an experienced pathologist, using microscopic features in pathology slides to assess cancer presence. Unlike a human observer, however, the model leverages vast amounts of data to digitally encode various pathological features, allowing it to quickly identify these characteristics in new images.

Model validation

A comprehensive evaluation of the model is conducted using cross-validation methods, such as k-fold cross-validation, to assess its stability and generalization capabilities. Model parameters are fine-tuned based on the evaluation results, implementing necessary optimization strategies to further enhance the accuracy and reliability of the model.

Performance evaluation of models

The models were evaluated using an independent test dataset. The evaluation included computing key performance metrics such as accuracy, recall, and F1 score to comprehensively assess the performance of the models in distinguishing the characteristics of the tumor microenvironment of different pathological subtypes of thyroid cancer.

Feature extraction and analysis

In this study, we extracted microenvironment-related features from thyroid cancer samples, including the interactions between tumor cells and immune cells (such as PD-L1 expression and the extent of immune cell infiltration) as well as the composition of the ECM (such as the density of collagen fibers). Deep learning techniques, specifically convolutional neural networks (CNN) and recurrent neural networks (RNN) were utilized to process and analyze pathological slide images as well as genetic and protein data. The model training process involved supervised learning with a considerable amount of labeled data, gradual adjustment of network parameters (such as learning rate and batch size), and the utilization of techniques like data augmentation to enhance the model's generalization ability. The extracted features were further analyzed using statistical methods (ANOVA) and data visualization tools (t-SNE, heatmap) to delve into the differentiation efficacy of the features among various pathological subtypes.

Evaluation of subtype discrimination efficacy

Methods such as cross-validation and receiver operating characteristic (ROC) curve analysis were employed to assess the performance of AI models in distinguishing pathological subtypes of thyroid cancer. Specifically, the dataset was divided into training and testing sets, and k-fold cross-validation was used during training to ensure the stability and reliability of the evaluation results. The model's performance was measured by calculating metrics such as accuracy, recall, and F1 score, which were based on the comparison between the model's predicted results and the actual annotated results.

Analysis of the relationship between microenvironment features and pathological subtypes

We utilized multivariate statistical analysis methods like logistic regression, decision trees, and support vector machines (SVM) to investigate the association between microenvironment features and pathological subtypes of thyroid cancer. These analyses helped assess the weight and significance of each feature in the model and identify the most influential features for differentiating between pathological subtypes. By comparing the contributions of different features to the model's classification efficacy, we were able to unveil which microenvironment features are closely related to specific pathological subtypes.

Independent sample validation

In order to verify the accuracy and generalization capability of the model, we conducted model validation using a separate testing dataset from the training dataset. Rigorous sample selection criteria and randomization processes were employed to ensure the representativeness and fairness of the testing set. The consistency between the model-predicted pathological subtypes and actual clinical diagnoses was compared using statistical tests (such as t-tests and chi-square tests) while also analyzing the differences in microenvironment features among different pathological subtypes.

Results

Efficient performance of AI models in thyroid cancer pathological subtype recognition

This study compared the performance of 10 AI algorithm models in recognizing pathological subtypes of thyroid cancer (Figure S3). The results indicate that the EfficientNetB0 model outperformed other models in several key metrics such as accuracy, recall rate, and F1 score, particularly showing high sensitivity and accuracy in distinguishing subtle pathological features. These findings suggest that the EfficientNetB0 model has a significant advantage in handling complex pathological image data.

The EfficientNetB0 model, unlike other algorithms in this study such as InceptionV4, DenseNet201, and VGG19, features unique design and performance optimizations:

Compound Scaling Strategy: EfficientNetB0's primary innovation is its compound scaling strategy, which optimizes depth, width, and resolution simultaneously. Unlike traditional CNNs, which often adjust only depth or width, this strategy enhances computational efficiency by finding an optimal network configuration under limited resources.

Parameter Efficiency: EfficientNetB0's lightweight design achieves high classification accuracy with fewer parameters and lower computational demand compared to complex models like InceptionV4 and DenseNet201, making it ideal for resource-limited devices.

Inverted Residual Blocks: EfficientNetB0 incorporates MobileNetV2's inverted residuals and ReLU6 activation, reducing complexity and addressing gradient vanishing. In contrast, VGG19's traditional convolutional blocks require more parameters and processing power.

Automated Architecture Search (NAS): EfficientNetB0 is designed through Neural Architecture Search (NAS), enabling automated, data-driven optimization. This differs from manually designed structures like InceptionV4 and DenseNet, allowing EfficientNet to balance efficiency and performance effectively.

Enhanced Generalization: The compound scaling and lightweight design of EfficientNetB0 improve generalization and reduce overfitting risk on benchmark tasks, while larger models, such as InceptionV4 and DenseNet201, may struggle with overfitting on small datasets.

EfficientNetB0 demonstrated significant advantages in the task of distinguishing between thyroid cancer and normal thyroid tissue. As shown in Fig. 1, the model achieved leading classification accuracy on the test set, demonstrating high sensitivity and accuracy in thyroid cancer diagnostics. Analysis across multiple performance metrics, including training accuracy, specificity, precision-recall curves, ROC curves, confusion matrix, and F1 score, further validated the outstanding performance of EfficientNetB0.

Firstly, the training accuracy curve in Fig. 1A shows that EfficientNetB0 rapidly reached over 94% accuracy within only two training epochs, indicating quick convergence. Specificity analysis in Fig. 1B reveals near-perfect specificity for normal samples and high specificity for cancer samples, indicating a low false-positive rate when identifying non-target classes, which is particularly suited for clinical diagnostics requiring high specificity.

Precision-recall and ROC curves in Fig. 1C and D further illustrate EfficientNetB0's classification capability. In regions of high recall, the model maintained high precision, reflecting robustness across classes. The ROC curve shows an AUC close to 1, indicating exceptional discriminatory ability between thyroid cancer and normal samples. The confusion matrix in Fig. 1E indicates a correct classification rate of 98% for the "cancer" class and 90% for the "normal" class, showcasing high accuracy across both categories. The F1 score in Fig. 1F also confirms the model's balanced precision and recall between "cancer" and "normal" classes, further supporting its reliability in real-world applications.

Additionally, the learning rate and training loss curves in Fig. 1G and H indicate that the model optimized gradually during training, achieving stable convergence by reducing the learning rate and minimizing training loss. The mean average precision (mAP) shown in Fig. 1I continued to increase, reflecting the model's comprehensive detection capability across multiple classes.

In summary, EfficientNetB0 outperformed other models in key performance metrics such as accuracy, recall, specificity, and F1 score, demonstrating exceptional expertise and applicability. It particularly excelled in handling complex thyroid cancer pathology image data. These results directly underscore the model's reliability and efficiency in practical application scenarios, supporting its potential for thyroid cancer diagnostics.

EfficientNetB0 model for accurate discrimination of four pathological subtypes of thyroid cancer

In the task of accurately distinguishing thyroid cancer pathological subtypes, the EfficientNetB0 model demonstrated outstanding performance, effectively identifying the four key subtypes: PTC, FTC, MTC, and ATC. Training accuracy improved consistently with each epoch, reaching around 90% by the sixth epoch, indicating effective convergence and successful feature learning specific to thyroid cancer subtypes (Fig. 2A).

The model achieved high specificity in differentiating between cancerous and normal samples, particularly excelling in the accurate identification of normal samples (Fig. 2B). This high specificity in excluding non-thyroid

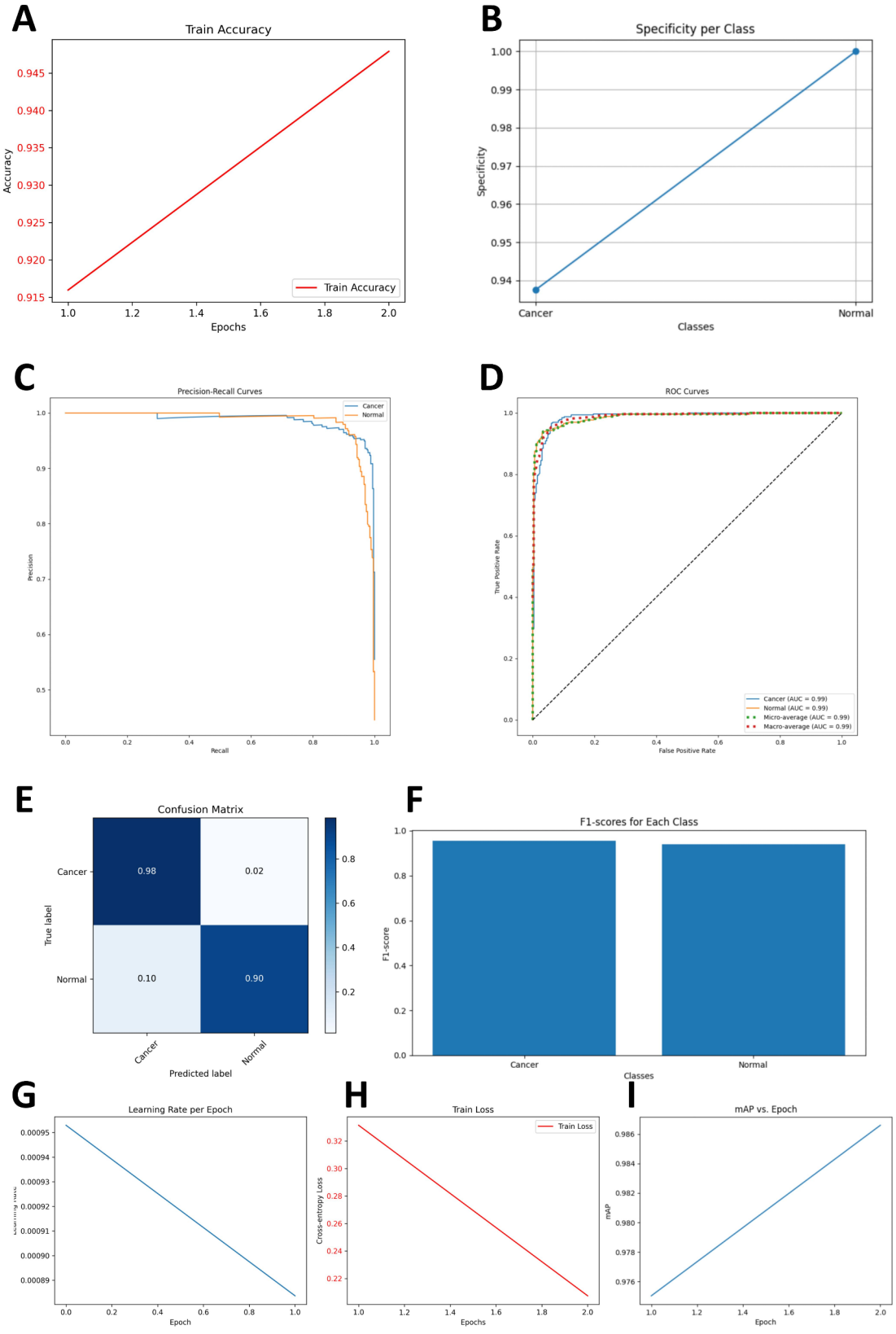

Fig. 1 Performance Demonstration of EfficientNetB0 Model in Discriminating Thyroid Cancer Tissue from Normal Thyroid Tissue. Note: (**A**) Diagnostic Accuracy; (**B**) Diagnostic Specificity; (**C**) Precision-Recall Curve; (**D**) ROC Curve; (**E**) Confusion Matrix; (**F**) F1 Scores; (**G**) Learning Rate; (**H**) Training Loss; (**I**) Mean Average Precision (mAP)

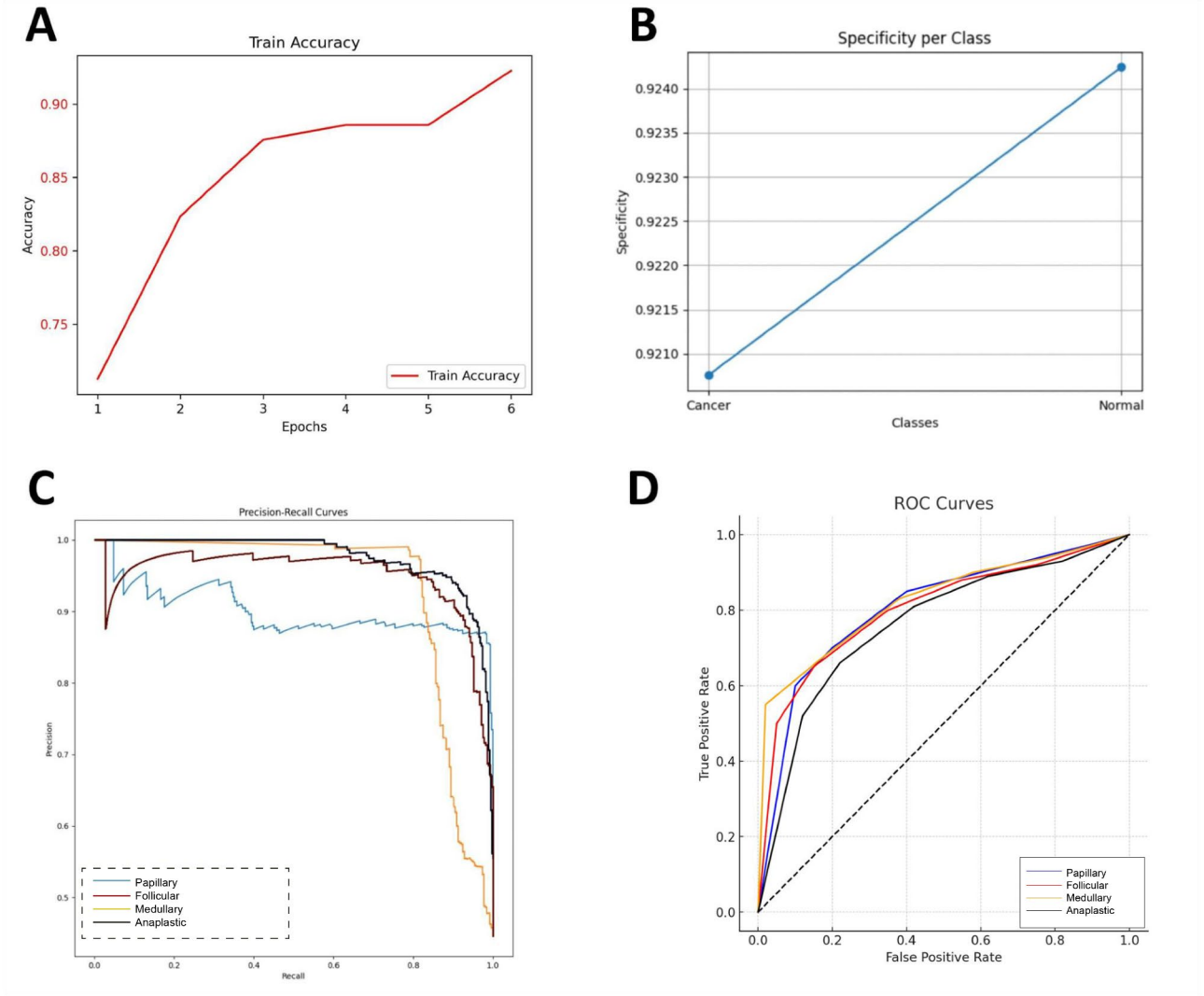

Fig. 2 Efficacy of EfficientNetB0 Model in Distinguishing Thyroid Cancer Pathological Subtypes.Note: (**A**) Classification Accuracy; (**B**) Classification Specificity; (**C**) Precision-Recall Curve; (**D**) ROC Curve

cancer samples contributed to a reduced false-positive rate, enhancing diagnostic reliability.

The precision-recall curves for the four thyroid cancer subtypes (Fig. 2C), illustrate varying classification difficulties among subtypes. For ATC, the precision decreases rapidly at high recall rates, indicating a greater challenge in classification, while the other subtypes maintain a more balanced relationship between precision and recall.

The ROC curves indicate that the model's discrimination ability is consistently strong across all subtypes, with each curve positioned above the random classification line (Fig. 2D). High AUC values, particularly for follicular and medullary carcinomas, confirm the model's robust classification accuracy and excellent differentiation capability.

In conclusion, the EfficientNetB0 model showed exceptional performance in classifying thyroid cancer subtypes, achieving high accuracy, particularly in recognizing common subtypes such as papillary and follicular. These results underscore the model's potential for precise diagnostic applications in thyroid cancer.

Performance analysis of the efficientNetB0 model in distinguishing the microenvironment features of pathological subtypes in thyroid cancer

The interaction between tumor and immune cells across different thyroid cancer subtypes shows that papillary subtypes exhibit the highest tumor-immune interaction level, while the anaplastic subtype shows the lowest. (Fig. 3A). The ECM component densities for each pathological subtype reveal that anaplastic subtypes generally have higher ECM component densities, whereas papillary subtypes are lower. This variation may impact tumor invasiveness and metastatic potential (Fig. 3B). The

A

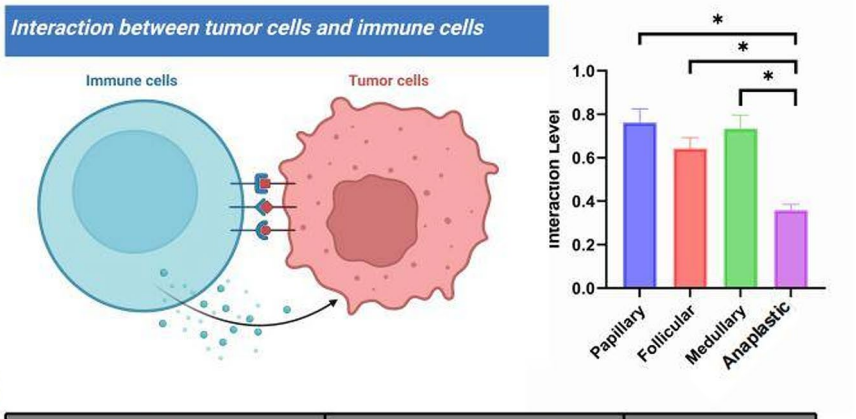

B

Subtype	ECM Component	Density
Papillary	Collagen IV Density	0.50
	Fibronectin Density	0.55
	Laminin Density	0.45
	Hyaluronan Density	0.60
Follicular	Collagen IV Density	0.80
	Fibronectin Density	0.62
	Laminin Density	0.58
	Hyaluronan Density	0.75
Medullary	Collagen IV Density	0.60
	Fibronectin Density	0.65
	Laminin Density	0.50
	Hyaluronan Density	0.68
Anaplastic	Collagen IV Density	0.90
	Fibronectin Density	0.85
	Laminin Density	0.88
	Hyaluronan Density	0.92

C

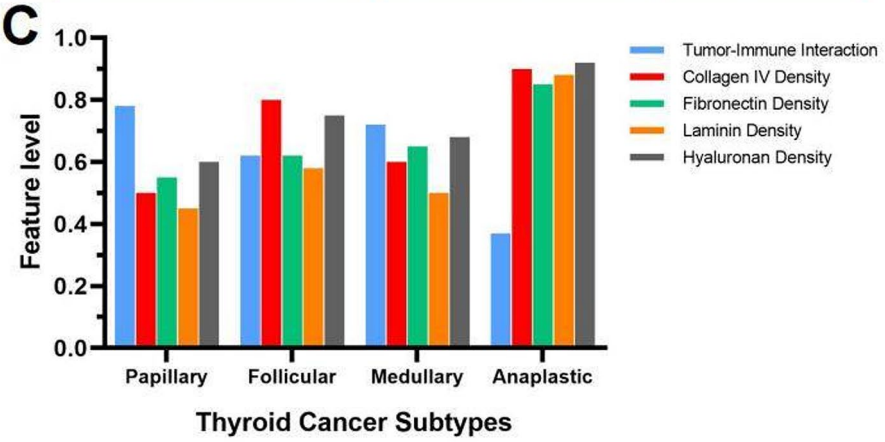

Fig. 3 Application of EfficientNetB0 Model in Analyzing Thyroid Cancer Microenvironment Features.Note: (**A**) Recognition of Interaction between Tumor Cells and Immune Cells; (**B**) Analysis of ECM Composition; (**C**) Comparative Analysis of Microenvironment Features among Different Pathological Subtypes

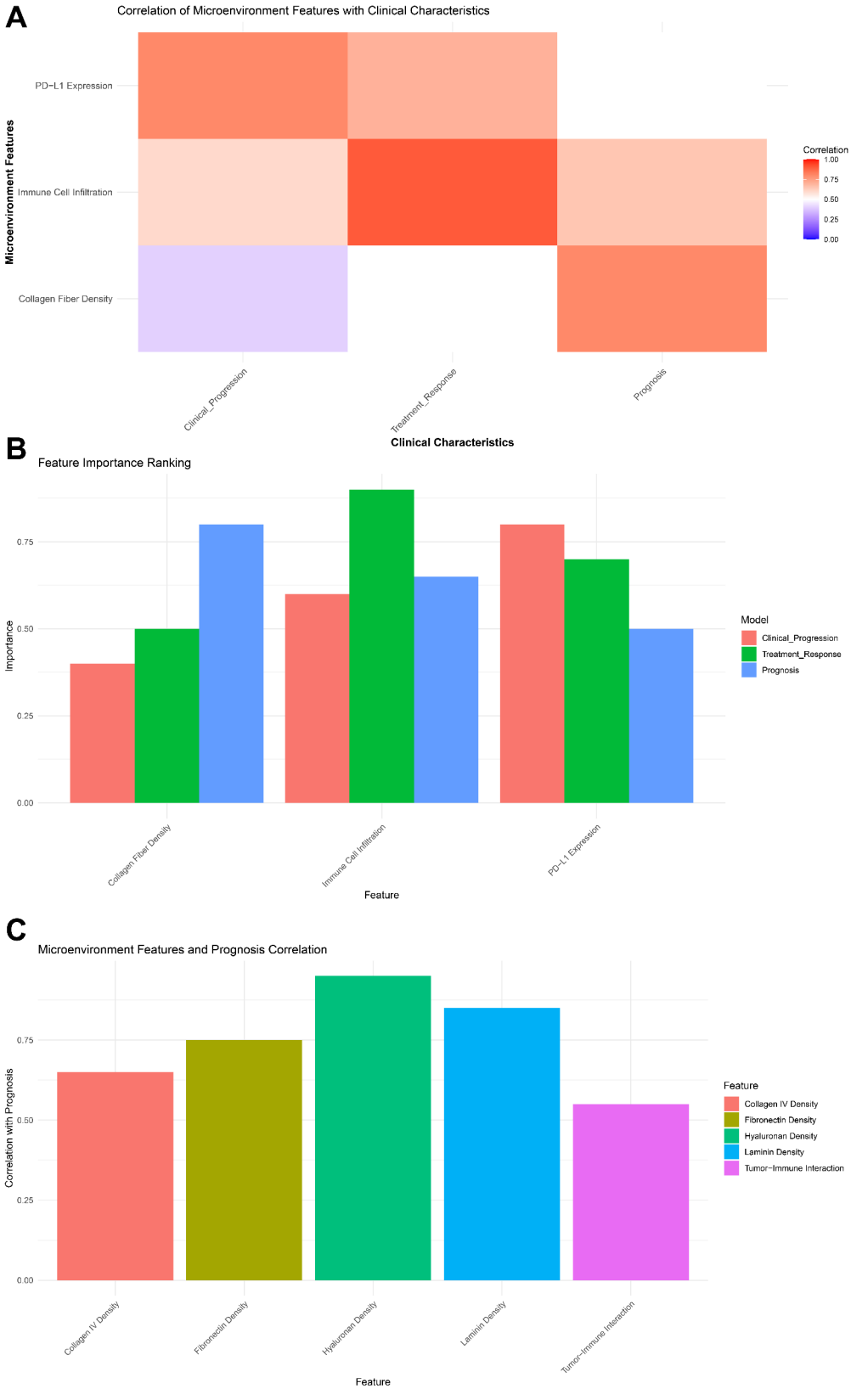

Fig. 4 (See legend on next page.)

(See figure on previous page.)

Fig. 4 Correlation Analysis Between Microenvironment Features and Clinical Progression of Thyroid Cancer. Note: (**A**) Correlation Heatmap between Microenvironment Features and Clinical Characteristics: Displays the correlation heatmap between different microenvironment features and clinical characteristics of thyroid cancer patients, such as disease progression and treatment response; (**B**) Ranking of Microenvironment Feature Importance: Demonstrates the ranking of the most influential microenvironment features for distinguishing thyroid cancer pathological subtypes based on multivariate statistical analysis methods like logistic regression, decision trees, and SVM; (**C**) Relationship Diagram between Microenvironment Features and Prognosis: Illustrates the relationship between specific microenvironment features and the prognosis of thyroid cancer patients

distribution trends of tumor-immune interactions and ECM component densities across subtypes indicate that anaplastic subtypes exhibit consistently higher feature levels, papillary subtypes lower, with follicular and medullary subtypes in between (Fig. 3C). These trends further support significant differences in microenvironmental features across pathological subtypes. The EfficientNetB0 model excels in distinguishing the tumor microenvironmental characteristics of thyroid cancer subtypes, and the identified differences in tumor-immune interaction and ECM component densities provide valuable insights into the biological properties of each subtype, offering a direction for further mechanistic studies.

The correlation between tumour microenvironment features and clinical progression of thyroid cancer

As shown in Fig. 4, the microenvironmental features identified by the EfficientNetB0 model are significantly correlated with clinical characteristics, treatment response, and prognosis in thyroid cancer. The heatmap in Fig. 4A illustrates the correlation between microenvironmental features (such as PD-L1 expression, immune cell infiltration, and collagen fiber density) and clinical characteristics (including clinical progression, treatment response, and prognosis). PD-L1 expression and immune cell infiltration show a strong positive correlation with treatment response and prognosis, while collagen fiber density exhibits a weaker correlation with clinical progression. These findings suggest that specific microenvironmental features may play distinct roles in the pathological development and clinical response of thyroid cancer.

The feature importance ranking in Fig. 4B displays the relative importance of various microenvironmental features across three models (clinical progression, treatment response, and prognosis). Immune cell infiltration is the most important feature in the treatment response model, while PD-L1 expression is important in the clinical progression models. Collagen fiber density shows higher importance in the prognosis model, indicating that different microenvironmental features contribute variably to clinical outcomes in thyroid cancer.

Figure 4C presents the correlation between different microenvironmental features and prognosis. Hyaluronan density demonstrates the highest correlation with prognosis. This suggests that certain ECM components may play critical roles in disease progression and prognosis in thyroid cancer.

In summary, the microenvironmental features identified by the EfficientNetB0 model, such as PD-L1 expression, immune cell infiltration, and ECM components, show significant associations with clinical characteristics and prognosis in thyroid cancer. Further analysis of the clinical relevance of these microenvironmental features can deepen the understanding of thyroid cancer biology and provide valuable insights for personalized treatment approaches.

Discussion

Thyroid cancer, a common malignancy of the endocrine system, has seen a significant increase in incidence over the past few decades [1–3]. The accurate identification of pathological subtypes is essential for devising personalized treatment strategies and evaluating prognosis. However, traditional pathological diagnostic methods have limitations [29–31]. Recent advancements in artificial intelligence and deep learning have significantly improved the analysis of medical imaging and molecular data, filling gaps in existing research and offering new perspectives for precise diagnosis and treatment [32–34].

This study differs from prior research in methodology. Earlier studies relied on traditional machine learning or early deep learning models, such as InceptionV4 and DenseNet201, which faced challenges in handling complex medical imaging data [35, 36]. In contrast, our study utilized EfficientNetB0, a model known for its superior performance in medical imaging tasks [37]. By comparing 10 AI models, EfficientNetB0 demonstrated higher accuracy and stability in identifying thyroid cancer subtypes, emphasizing the importance of selecting optimal deep learning models for improved diagnostic precision. And our comprehensive model comparison identified EfficientNetB0 as the best performer in distinguishing thyroid cancer subtypes and recognizing key microenvironmental features. Its optimized convolutional neural network significantly enhances classification accuracy and efficiency [38–40]. Large-scale datasets and cross-validation ensured the model's stability and generalizability [41]. EfficientNetB0 outperformed other models in classifying papillary, follicular, medullary, and anaplastic thyroid carcinoma subtypes based on accuracy, recall, and F1 score [5, 42, 43].

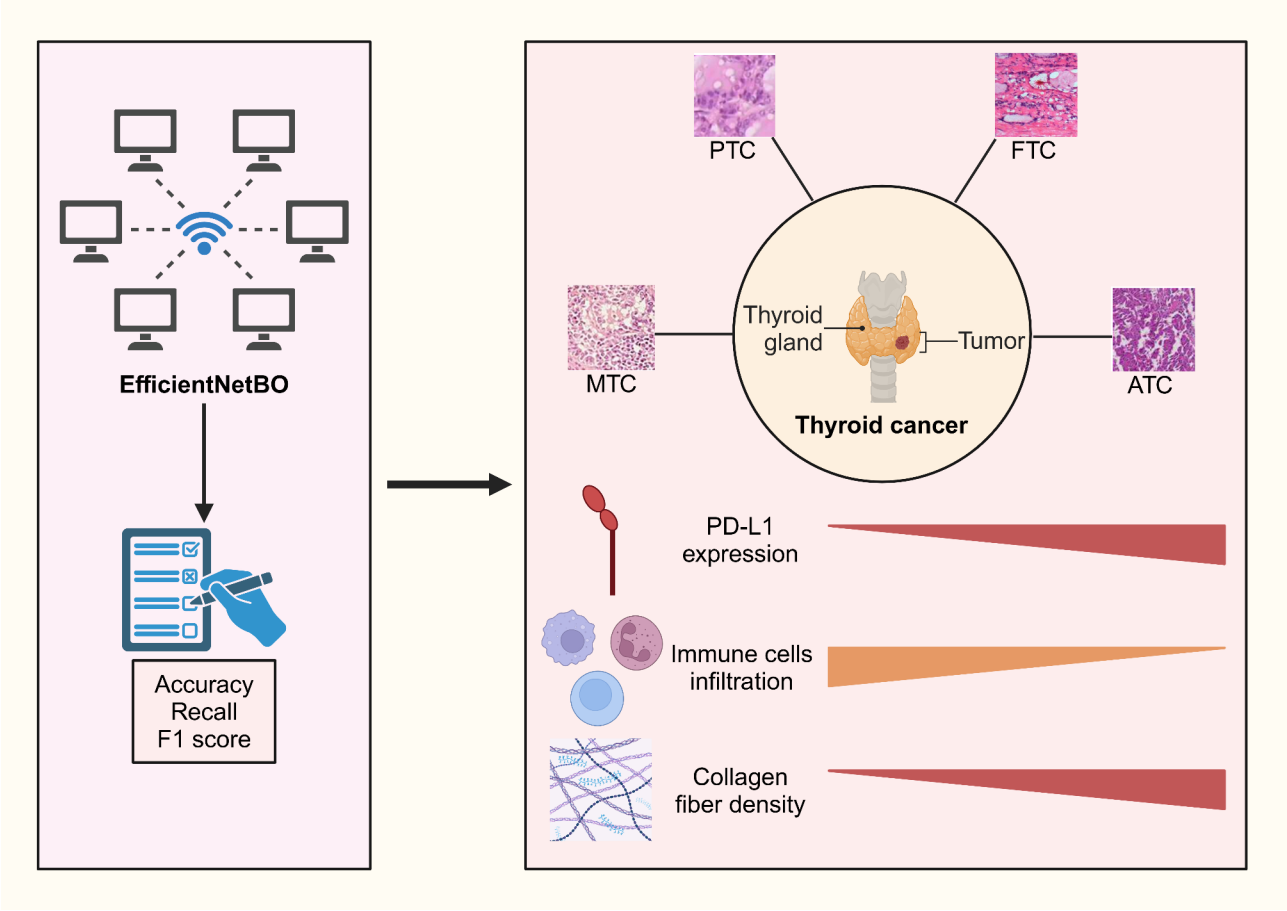

Fig. 5 Molecular Mechanism Diagram Depicting the Association of Thyroid Cancer Microenvironment Features with Pathological Subtypes

Beyond classification, EfficientNetB0 extracts and analyzes key microenvironmental features, such as tumor-immune cell interactions (PD-L1 expression, immune cell infiltration) and ECM components (collagen fiber density) [44, 45]. These features are essential for understanding thyroid cancer's biological behavior and clinical progression. This study highlights significant associations between microenvironmental features and pathological subtypes, demonstrating EfficientNetB0's potential for analyzing complex medical data. Our findings confirm the high efficiency and clinical applicability of EfficientNetB0 in thyroid cancer diagnostics and microenvironment analysis (Fig. 5). Compared to previous models, EfficientNetB0 offers significant advantages in diagnostic accuracy, sensitivity, and generalization capabilities. These results provide robust technical support for precise diagnosis and treatment while paving the way for AI applications in tumor pathology. However, challenges remain regarding model interpretability and adaptability across diverse populations, requiring further exploration.

This study has advanced the identification of thyroid cancer subtypes and analysis of tumor microenvironment features using the EfficientNetB0 model. The model's high-precision diagnostic capability allows for the extraction and analysis of key tumor microenvironment features, such as PD-L1 expression, immune cell infiltration, and collagen fiber density. These factors play a crucial role in understanding thyroid cancer's biological behavior, disease progression, and treatment response. Clinically, EfficientNetB0 enhances diagnostic accuracy, reduces misdiagnosis risks, and supports personalized treatment planning. By leveraging these microenvironmental insights, physicians can better assess prognosis and refine treatment strategies, particularly for immunotherapy, improving patient outcomes and quality of life.

Although this study has made significant progress, there are still some limitations. Firstly, the sample size is relatively small, consisting of only 118 cases of thyroid cancer patients, which may restrict the model's generalizability and the universality of the results. Secondly, the data is sourced solely from affiliated hospitals, potentially introducing selection bias and failing to comprehensively represent the situations across different regions and medical institutions. Additionally, while the EfficientNetB0 model performed well in this study, its stability and reliability in practical clinical applications still require

further validation, especially when handling more diverse and complex cases. Finally, this study primarily focuses on the analysis of imaging and molecular data, and future research should incorporate more clinical variables, such as patients' medical histories and treatment records, to enhance the model's comprehensive analytical capabilities and clinical utility.

Future research should expand sample sizes and include data from more diverse medical institutions to improve model applicability. Further optimization and validation of EfficientNetB0 are necessary to ensure its stability and reliability in clinical practice. Integrating a broader range of clinical data, including patient histories, treatment responses, and quality of life assessments, will facilitate a more comprehensive understanding of thyroid cancer mechanisms. Additionally, exploring EfficientNetB0's potential application in other cancer types could lead to universal AI-driven diagnostic tools. As AI technology advances and data availability grows, future studies are expected to drive innovations in precision medicine and personalized cancer treatment.

Supplementary Information

The online version contains supplementary material available at https://doi.org/10.1186/s13000-025-01621-6 .

Supplementary Material 1

Supplementary Material 2

Supplementary Material 3

Supplementary Material 4

Acknowledgements
None.

Author contributions
Hongpeng Guo and Junjie Zhang designed the study and contributed equally to the conceptualization and methodology development. You Li and Xinghe Pan were responsible for data collection, preprocessing, and analysis of pathological tissue samples. Chenglin Sun performed the data validation and contributed to the evaluation of the AI models, particularly the EfficientNetB0 model. All authors contributed to writing, reviewing, and editing the manuscript. Chenglin Sun and Xinghe Pan supervised the research and were the primary contacts for correspondence.

Funding
This study was supported by Liaoning Provincial Science and Technology Plan project (Grant no.2022JH2/1013), the Shenyang Science and Technology Plan Project (Grant no.21173918),the Graduate Student Science and Technology Innovation Fund of Shenyang Medical College (Grant no. Y20220531) and Shenyang Health Commission Scientific Research Project (Grant no. 202358).

Data availability
All data can be provided as needed.

Declarations

Ethical approval
This study was approved by the Clinical Ethics Committee of Central Hospital Affiliated to Shenyang Medical College (Section-2023-007).

Competing interests
The authors declare no competing interests.

Received: 11 July 2024 / Accepted: 18 February 2025
Published online: 07 March 2025

References

1. Morton LM, Karyadi DM, Stewart C, et al. Radiation-related genomic profile of papillary thyroid carcinoma after the Chernobyl accident. Science. 2021;372(6543):eabg2538. https://doi.org/10.1126/science.abg2538.
2. Acuña-Ruiz A, Carrasco-López C, Santisteban P. Genomic and epigenomic profile of thyroid cancer. Best Pract Res Clin Endocrinol Metab. 2023;37(1):101656. https://doi.org/10.1016/j.beem.2022.101656.
3. Kosák M. Endocrine late effects of cancer treatment. Pozdní endokrinologické komplikace onkologické léčby. Klin Onkol. 2021;34(6):440–449. doi:10.48095/ccko2021440lF: NA NA NA.
4. Jung CK, Bychkov A, Kakudo K. Update from the 2022 world health organization classification of thyroid tumors: A standardized diagnostic approach. Endocrinol Metab (Seoul). 2022;37(5):703–18. https://doi.org/10.3803/EnM.2022.1553.
5. Baloch ZW, Asa SL, Barletta JA, et al. Overview of the 2022 WHO classification of thyroid neoplasms. Endocr Pathol. 2022;33(1):27–63. https://doi.org/10.1007/s12022-022-09707-3.
6. Liu SQ, Gao ZJ, Wu J et al. Single-cell and spatially resolved analysis uncovers cell heterogeneity of breast cancer. J Hematol Oncol. 2022;15(1):19. Published 2022 Mar 3. https://doi.org/10.1186/s13045-022-01236-0
7. Boucai L, Zafereo M, Cabanillas ME, Thyroid Cancer. Rev JAMA. 2024;331(5):425–35. https://doi.org/10.1001/jama.2023.26348.
8. Lu D, Yang J, Liu X, et al. Clinicopathological features, survival outcomes, and appropriate surgical approaches for stage I acinar and papillary predominant lung adenocarcinoma. Cancer Med. 2020;9(10):3455–62. https://doi.org/10.1002/cam4.3012.
9. Pu W, Shi X, Yu P et al. Single-cell transcriptomic analysis of the tumor ecosystems underlying initiation and progression of papillary thyroid carcinoma. Nat Commun. 2021;12(1):6058. Published 2021 Oct 18. https://doi.org/10.1038/s41467-021-26343-3
10. Ham J, Wang B, Po JW, Singh A, Niles N, Lee CS. Cancer-associated fibroblasts (CAFs) in thyroid papillary carcinoma: molecular networks and interactions. J Clin Pathol. 2021;74(12):759–65. https://doi.org/10.1136/jclinpath-2020-207357.
11. Han PZ, Ye WD, Yu PC, et al. A distinct tumor microenvironment makes anaplastic thyroid cancer more lethal but immunotherapy sensitive than papillary thyroid cancer. JCI Insight. 2024;9(8):e173712. https://doi.org/10.1172/jci.insight.173712. Published 2024 Mar 7.
12. Blaivas M, Blaivas L. Are all deep learning architectures alike for Point-of-Care ultrasound?? Evidence from a cardiac image classification model suggests otherwise. J Ultrasound Med. 2020;39(6):1187–94. https://doi.org/10.1002/jum.15206.
13. Pattarone G, Acion L, Simian M, Mertelsmann R, Follo M, Iarussi E. Learning deep features for dead and living breast cancer cell classification without staining [published correction appears in Sci Rep. 2021;11(1):19442. doi: 10.1038/s41598-021-99144-9]. Sci Rep. 2021;11(1):10304. Published 2021 May 13. https://doi.org/10.1038/s41598-021-89895-w
14. Wu F, Yang H, Peng L, et al. AGNet: automatic generation network for skin imaging reports. Comput Biol Med. 2022;141:105037. https://doi.org/10.1016/j.compbiomed.2021.105037.
15. Kussaibi H, Alsafwani N. Trends in AI-powered classification of thyroid neoplasms based on histopathology Images - a systematic review. Acta Inf Med. 2023;31(4):280–6. https://doi.org/10.5455/aim.2023.31.280-286.
16. Haq F, Park G, Jeon S, Hirokawa M, Jung CK. Utilizing Immunoglobulin G4 immunohistochemistry for risk stratification in patients with papillary thyroid carcinoma associated with Hashimoto thyroiditis. Endocrinol Metab (Seoul). 2024;39(3):468–78. https://doi.org/10.3803/EnM.2024.1923.
17. Zhou J, Zhang Y, Chang KT, et al. Diagnosis of benign and malignant breast lesions on DCE-MRI by using radiomics and deep learning with consideration of peritumor tissue. J Magn Reson Imaging. 2020;51(3):798–809. https://doi.org/10.1002/jmri.26981.
18. Yu M, Zhang S. Influenced tumor microenvironment and tumor immunity by amino acids. Front Immunol. 2023;14:1118448. https://doi.org/10.3389/fimmu.2023.1118448. Published 2023 Jan 31.

19. Siminzar P, Tohidkia MR, Eppard E, Vahidfar N, Tarighatnia A, Aghanejad A. Recent trends in diagnostic biomarkers of tumor microenvironment. Mol Imaging Biol. 2023;25(3):464–82. https://doi.org/10.1007/s11307-022-01795-1.
20. Xiang Y, Miao H. Lipid metabolism in Tumor-Associated macrophages. Adv Exp Med Biol. 2021;1316:87–101. https://doi.org/10.1007/978-981-33-6785-2_6.
21. Dai SM, Li FJ, Long HZ, et al. Relationship between MiRNA and ferroptosis in tumors. Front Pharmacol. 2022;13:977062. https://doi.org/10.3389/fphar.2022.977062. Published 2022 Nov 4.
22. Wang Q, Zhi Y, Zi M, et al. Spatially resolved transcriptomics technology facilitates Cancer research. Adv Sci (Weinh). 2023;10(30):e2302558. https://doi.org/10.1002/advs.202302558.
23. Chen X, Wang K, Jiang S, et al. eEF2K promotes PD-L1 stabilization through inactivating GSK3β in melanoma. J Immunother Cancer. 2022;10(3):e004026. https://doi.org/10.1136/jitc-2021-004026.
24. Sun Z, Mai H, Xue C, et al. Hsa-LINC02418/mmu-4930573I07Rik regulated by METTL3 dictates anti-PD-L1 immunotherapeutic efficacy via enhancement of Trim21-mediated PD-L1 ubiquitination. J Immunother Cancer. 2023;11(12):e007415. https://doi.org/10.1136/jitc-2023-007415. Published 2023 Dec 1.
25. Pusztaszeri MP, Bongiovanni M, Brimo F. Do we need PD-L1 as a biomarker for thyroid cytologic and histologic specimens? Cancer Cytopathol. 2020;128(3):160–5. https://doi.org/10.1002/cncy.22223.
26. Lin YY, Lin LY, Hang JF, Lin CH, Ho HL, Chou TY. Programmed death-ligand 1 (PD-L1)/thyroid transcription factor-1 double immunohistochemical staining facilitates scoring of tumor PD-L1 expression in cytopathology specimens from lung adenocarcinoma patients. Cancer Cytopathol. 2021;129(2):148–55. https://doi.org/10.1002/cncy.22359.
27. Shobab L, Burman KD, Wartofsky L. Sex differences in differentiated thyroid Cancer. Thyroid. 2022;32(3):224–35. https://doi.org/10.1089/thy.2021.0361.
28. Jayasinghe R, Basnayake O, Jayarajah U, Seneviratne S. Management of medullary carcinoma of the thyroid: a review. J Int Med Res. 2022;50(7):3000605221110698. https://doi.org/10.1177/03000605221110698.
29. Li Q, Zhu F, Xiao Y, et al. Synchronous double primary lymphoma and thyroid cancer: A single-institution retrospective study. Med (Baltim). 2021;100(39):e27061. https://doi.org/10.1097/MD.0000000000027061.
30. Shang X, Hu B, Gao F, Ren W. Correlation between computed tomography imaging and pathological stages and subtypes in early lung adenocarcinoma. J Cancer Res Ther. 2020;16(7):1569–74. https://doi.org/10.4103/jcrt.JCRT_726_20.
31. Wu SS, Lamarre ED, Yalamanchali A, et al. Association of treatment strategies and tumor characteristics with overall survival among patients with anaplastic thyroid cancer: A Single-Institution 21-Year experience. JAMA Otolaryngol Head Neck Surg. 2023;149(4):300–9. https://doi.org/10.1001/jamaoto.2022.5045.
32. Shen YT, Chen L, Yue WW, Xu HX. Artificial intelligence in ultrasound. Eur J Radiol. 2021;139:109717. https://doi.org/10.1016/j.ejrad.2021.109717.
33. Zhang Q, Zhang S, Pan Y, et al. Deep learning to diagnose Hashimoto's thyroiditis from sonographic images. Nat Commun. 2022;13(1):3759. https://doi.org/10.1038/s41467-022-31449-3. Published 2022 Jun 29.
34. Cao CL, Li QL, Tong J, et al. Artificial intelligence in thyroid ultrasound. Front Oncol. 2023;13:1060702. https://doi.org/10.3389/fonc.2023.1060702. Published 2023 May 12.
35. Emmitt J, Masoud-Ansari S, Phillipps R, Middleton S, Graydon J, Holdaway S. Machine learning for stone artifact identification: distinguishing worked stone artifacts from natural clasts using deep neural networks. PLoS ONE. 2022;17(8):e0271582. https://doi.org/10.1371/journal.pone.0271582. Published 2022 Aug 10.
36. Yang S, Hu Y, Wang X, et al. Machine learning and deep learning to identifying subarachnoid haemorrhage macrophage-associated biomarkers by bulk and single-cell sequencing. J Cell Mol Med. 2024;28(9):e18296. https://doi.org/10.1111/jcmm.18296.
37. Sambyal AS, Niyaz U, Krishnan NC, Bathula DR. Understanding calibration of deep neural networks for medical image classification. Comput Methods Programs Biomed. 2023;242:107816. https://doi.org/10.1016/j.cmpb.2023.107816.
38. Elizar E, Zulkifley MA, Muharar R, Zaman MHM, Mustaza SM. A Review on Multiscale-Deep-Learning Applications. Sensors (Basel). 2022;22(19):7384. Published 2022 Sep 28. https://doi.org/10.3390/s22197384
39. Sundell VM, Mäkelä T, Vitikainen AM, Kaasalainen T. Convolutional neural network -based Phantom image scoring for mammography quality control. BMC Med Imaging. 2022;22(1):216. https://doi.org/10.1186/s12880-022-00944-w. Published 2022 Dec 7.
40. Zhang L, Zhang J, Gao S. Region-Based convolutional neural Network-Based spine model positioning of X-Ray images. Biomed Res Int. 2022. https://doi.org/10.1155/2022/7512445. 2022:7512445. Published 2022 Jun 17.
41. Coley RY, Liao Q, Simon N, Shortreed SM. Empirical evaluation of internal validation methods for prediction in large-scale clinical data with rare-event outcomes: a case study in suicide risk prediction. BMC Med Res Methodol. 2023;23(1):33. Published 2023 Feb 1. https://doi.org/10.1186/s12874-023-01844-5
42. Zheng C, Wang W, Young SD. Identifying HIV-related digital social influencers using an iterative deep learning approach. AIDS. 2021;35(Suppl 1):S85–9. https://doi.org/10.1097/QAD.0000000000002841.
43. Rudolph AE, Young AM. Privacy and confidentiality considerations for collecting HIV risk network data among men who have sex with men and implications for constructing valid risk networks. Soc Networks. 2021;67:47–54. https://doi.org/10.1016/j.socnet.2019.09.002.
44. Hajjarian Z, Brachtel EF, Tshikudi DM, Nadkarni SK. Mapping mechanical properties of the tumor microenvironment by laser speckle rheological microscopy. Cancer Res. 2021;81(18):4874–85. https://doi.org/10.1158/0008-5472.CAN-20-3898.
45. Lv SQ, Fu Z, Yang L, et al. Comprehensive omics analyses profile genesets related with tumor heterogeneity of multifocal glioblastomas and reveal LIF/CCL2 as biomarkers for mesenchymal subtype. Theranostics. 2022;12(1):459–73. https://doi.org/10.7150/thno.65739. Published 2022 Jan 1.

Publisher's note